

Towards Scalable Foundation Models for Digital Dermatology

Fabian Gröger^{1,2}

Philippe Gottfrois¹

Ludovic Amruthalingam²

Alvaro Gonzalez-Jimenez¹

Simone Lionetti²

Luis R. Soenksen-Martinez^{4,5}

Alexander A. Navarini^{*1,3}

Marc Pouly^{*2}

FABIAN.GROEGER@UNIBAS.CH

PHILIPPE.GOTTFROIS@UNIBAS.CH

LUDOVIC.AMRUTHALINGAM@HSLU.CH

ALVARO.GONZALEZJIMENEZ@UNIBAS.CH

SIMONE.LIONETTI@HSLU.CH

SOENKSEN@MIT.EDU

ALEXANDER.NAVARINI@USB.CH

MARC.POULY@HSLU.CH

¹*Department of Biomedical Engineering, University of Basel, Switzerland*

²*Department of Computer Science, Lucerne University of Applied Sciences and Arts, Switzerland*

³*Department of Dermatology, University Hospital of Basel, Switzerland*

⁴*J-Clinic for AI and Health, Massachusetts Institute of Technology, USA*

⁵*Center for Bioengineering Innovation and Design, Johns Hopkins University, USA*

Abstract

The growing demand for accurate and equitable AI models in digital dermatology faces a significant challenge: the lack of diverse, high-quality labeled data. In this work, we investigate the potential of domain-specific foundation models for dermatology in addressing this challenge. We utilize self-supervised learning (SSL) techniques to pre-train models on a dataset of over 240,000 dermatological images from public and private collections. Our study considers several SSL methods and compares the resulting foundation models against domain-agnostic models like those pre-trained on ImageNet and state-of-the-art models such as MONET across 12 downstream tasks. Unlike previous research, we emphasize the development of smaller models that are more suitable for resource-limited clinical settings, facilitating easier adaptation to a broad range of use cases. Results show that models pre-trained in this work not only outperform general-purpose models but also approach the performance of models 50 times larger on clinically relevant diagnostic tasks. To promote further research in this direction, we publicly release both the training code and the foundation models, which can benefit clinicians in dermatological applications.

Keywords: Foundation model, Self-supervised learning, Digital dermatology.

Data and Code Availability. Datasets used for evaluation are publicly accessible and detailed in Appendix B. Code and models to reproduce the results are available¹. Together this ensures full reproducibility of the evaluation results.

Institutional Review Board (IRB). IRB approval is not required for our research, as it utilizes existing datasets and involves no direct interaction with human subjects beyond the use of previously collected human annotations.

1. Introduction

The scarcity of high-quality, large-scale annotated data remains a significant challenge in the medical field (Arora et al., 2023). This is due to the high costs of expert annotations (Castro et al., 2020), difficulties in reaching consensus among experts (Jacob et al., 2021), data imbalance due to rare conditions, biases in data collection (Groh et al., 2021), and legal constraints on the annotation process. Transfer learning from models pre-trained on natural images such as ImageNet has become standard practice to address data scarcity (Baykal et al., 2020). Recently, foundation models—deep learning models trained on vast amounts of unlabeled data—have gained interest for their adaptability across a wide range of tasks (Awais et al., 2023). Domain-specific foundation models have

* Joint last authorship.

1. <https://github.com/Digital-Dermatology/self-supervised-dermatology>

received particular attention in the medical field since they tend to outperform their domain-agnostic counterparts (Azad et al., 2023). Smaller foundation models are also valuable for their ease of deployment and accessibility, enabling advanced tools to be used even in resource-constrained settings (Touvron et al., 2023). Although some domains such as histopathology (Lu et al., 2024), radiology (Wu et al., 2023), or ophthalmology (Zhou et al., 2023) have seen great progress in this direction, dermatology is lagging behind (Azad et al., 2023). Given the visual diversity of skin conditions and the need for equitable representation across skin tones, tailored foundation models could significantly improve both diagnostic accuracy and fairness in digital dermatology.

This paper presents preliminary results from the development of image-based foundation models for dermatology that are optimized for both efficiency and widespread accessibility. We focus on identifying the pre-training methodology that yields the best-performing model across 12 clinically relevant downstream tasks evaluated in terms of their frozen and low-data performance. Additionally, we release the models for the community to use, including training and evaluation scripts.

2. Related Work

The progress of foundation models is based on two key advancements: the availability of large-scale datasets and the development of learning techniques capable of training models without relying on labeled data, such as with self-supervised learning (SSL). This technique has gained popularity in the medical field because large unlabeled datasets are generally more accessible than their annotated counterparts (Azad et al., 2023). The idea of SSL is to learn data representations using an artificial supervised objective, often called the *pretext task*, created from a pool of unlabeled data. Representations are then generally assessed through *downstream tasks* and can be used to solve relevant tasks, where annotated data are available but potentially scarce. In recent years, SSL has been widely used to learn meaningful visual foundation models without relying on manual annotations across medical disciplines (Lu et al., 2024; Wu et al., 2023; Zhou et al., 2023). For a comprehensive review of SSL we refer to Liu et al. (2021) and to Shurrab and Duwairi (2022) focusing specifically on medical applications. The following section introduces the SSL methods used in this work.

Many SSL methods focus on discriminative approaches, where each image is considered a separate class, and the objective is to tell them apart. SimCLR (Chen et al., 2020) is a prominent example, which uses a contrastive loss to compare different views of the same image against other randomly sampled images. A caveat of this approach is that it requires comparing features from numerous images simultaneously, which demands large batch sizes. BYOL (Grill et al., 2020) is a popular method circumventing this issue with a carefully implemented asymmetric student-teacher architecture. Similarly, DINO (Caron et al., 2021) compares probability-like outputs from different patches of the same image using a teacher and a student network, prominently leveraging a vision transformer (ViT) (Dosovitskiy, 2020) and a multi-crop augmentation strategy. iBOT (Zhou et al., 2022) further builds on these ideas and explicitly exploits inherent properties of ViTs to capture both local and global information. Other approaches use paired multi-modal data for pre-training. For instance, CLIP (Radford et al., 2021) aligns visual and textual representations with a contrastive objective, jointly training image and text encoders that can be independently utilized post-training.

3. Methodology

Pre-training Data. We curated a collection of unlabeled dermatology pictures from public and private sources, totaling 242,039 images. The collection includes modalities typically used in digital dermatology, namely dermoscopy and clinical images. The datasets used for pre-training are listed in Appendix A, and include MED-NODE (Giotis et al., 2015), PH² (Mendonça et al., 2013), SD-260 (Sun et al., 2016a), ISIC (ISIC, 2016), and a private collection from the University Hospital of Basel.

Downstream Tasks. We use 9 datasets for evaluation: MED-NODE (Giotis et al., 2015), PH² (Mendonça et al., 2013), DDI (Daneshjou et al., 2022), Derm7pt (Kawahara et al., 2019), PAD-UFES-20 (Pacheco et al., 2020), SD-128 (Sun et al., 2016b), PASSION (Gottfrois et al., 2024), HAM10000 (Tschandl et al., 2018), and Fitzpatrick17k (Groh et al., 2021). This results in a total of 12 diagnostic downstream tasks. Some of the datasets purposely overlap with the pre-training data, whereas others do not, to compare general-

ization beyond the seen collection. The downstream tasks were selected to represent common challenges in dermatology, such as different image modalities (clinical and dermoscopy images), different Fitzpatrick skin types, and small sample counts. More details on the downstream tasks can be found in Appendix B.

Final evaluations are performed on the test set provided by the dataset authors when available. When no designated test set is provided, we set apart 15% of the original data for testing. For datasets without a predefined validation set, we also split the data not used for testing into 85%/15% for training and validation. Splits are performed at patient level whenever possible. Additionally, we remove quality issues identified by SelfClean (Gröger et al., 2023; Gröger et al., 2024) to enhance the reliability of the performance estimates.

Implementation. The foundation models in this work can be divided into two groups based on their encoder architecture, which is either a CNN or a ViT. To promote comparability between the groups, we selected architectures with similar performance on ImageNet. For the CNN-based models, we use ResNet-50 (He et al., 2016), while for the ViT-based models, we choose ViT-Tiny (ViT-T) (Dosovitskiy, 2020) with a 16×16 patch size. ResNet-50 has approximately 23 million trainable parameters, and ViT-T has 5 million. Model configurations, including method-specific parameters and augmentation techniques, were initially taken from the original works. We then ensured that all models converged to suitable solutions by manually tuning the optimizer, learning rate, and method-specific hyperparameters. Final configurations can be found in table 1. Model inputs are resized to 224×224 pixels and normalized using the mean and standard deviation of ImageNet (Deng et al., 2009). All models were trained until the validation loss did not improve consecutively over twenty epochs.

The implementation is based on PyTorch (Paszke et al., 2019) and the official repositories of the selected SSL methods. Experiments are performed on a Nvidia DGX station, which features eight V100 GPUs, each with 32 GB of memory, 512 GB of system memory, and a CPU with 40 cores.

Training and Evaluation Protocols. All models are evaluated on a suite of downstream tasks, adhering to standard practice in SSL (Xu et al., 2024). Specifically, performance is computed with frozen features using both linear and k -nearest neighbor (kNN)

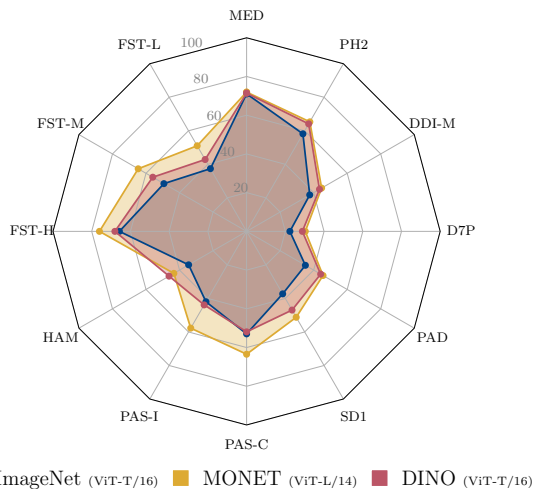


Figure 1: Macro-averaged test F1 for frozen kNN evaluation of the best-performing foundation model, domain-agnostic ImageNet model, and MONET for dermatological diagnostic tasks. Consult Appendix B for task details and D for more detailed results.

models. Frozen evaluation examines how well representations separate a dataset attribute, indicating whether inherent properties of the downstream task were learned during pre-training, relying solely on visual information. To further assess the models’ effectiveness in low-data scenarios, we train linear and kNN classifiers on randomly selected subsets of labeled data with increasing size and evaluate them all on the same test set.

We compare the domain-specific foundation models against domain-agnostic models pre-trained on ImageNet with supervision, specifically a ResNet-50 and ViT-T. Additionally, to estimate state-of-the-art performance for downstream tasks, regardless of model size or additional information used, we compare against MONET (Kim et al., 2024), an image-text foundation model trained on 105,550 dermatological images paired with natural language descriptions from medical literature. MONET is pre-trained using CLIP and uses a ViT-L image encoder with a 14×14 patch size, containing 304 million parameters, significantly larger than the other models compared in this work. Moreover, it requires significantly more FLOPs than the considered models in this paper (61.6×10^9 vs. 1.3×10^9) and has slower inference (277 vs. 3796 im/s) (Touvron et al., 2022).

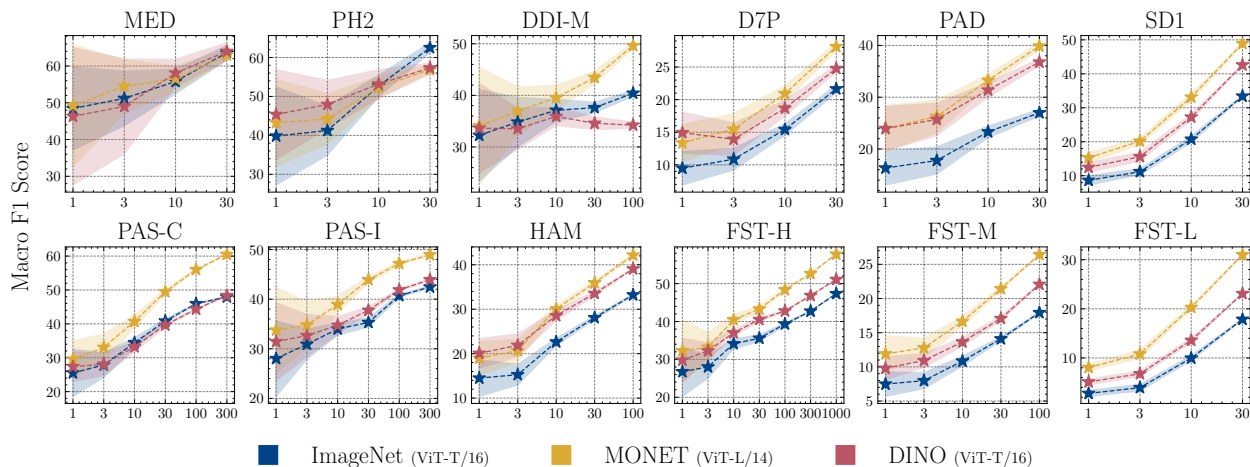


Figure 2: Results of a kNN classifier on pre-trained representations when varying the number of training samples per class available for downstream tasks. Performance is obtained by repeating the sampling process 50 times and reporting the average and standard errors.

4. Results

In figure 1, we compare foundation models pre-trained using diverse methods on a suite of downstream tasks in terms of frozen kNN performance. Specifically, we compare the best-performing foundation model trained in this paper, here a DINO pre-trained ViT-T, with the best-performing domain-agnostic model, here a ViT-T supervised pre-trained on ImageNet, and an estimation of the current state-of-the-art through MONET’s performance. Results are obtained by repeating the evaluation with five random seeds and reporting average performance. Detailed results for kNN and linear evaluation can be found in table 2 of the appendix. Here we explicitly focus on kNN performance since this correlates better with fine-tuned performance and is more robust to hyperparameter choices (Caron et al., 2021).

The DINO foundation model performs better in most tasks compared to the domain-agnostic ImageNet model, and is on par with state-of-the-art performance for half of the tasks. The performance gap between DINO and state-of-the-art is most noticeable for PAS-I and PAS-C, which are very difficult. Indeed, these only contain non-standardized, pigment-rich patients, of which the models pre-trained in this paper have seen limited amounts. However, for other tasks that also did not overlap with the pre-training dataset, the model is generalizing well, including for those featuring pigment-rich skin, such as DDI-M,

FST-H, FST-M, and FST-L. When investigating different SSL strategies in table 2, we find that most, except for iBOT, fall short of similar performance. In conclusion, we observe that even models significantly smaller than MONET can achieve state-of-the-art performance with appropriate pre-training, such as DINO or iBOT.

In figure 2, we compare different foundation models by adding a kNN classifier on frozen features and varying the training dataset size for the downstream tasks. The same experiment with a linear classifier can be found in figure 4 of the appendix. Results show that across the majority of tasks, the domain-specific DINO model performs better than the supervised domain-agnostic ImageNet model. Additionally, for some tasks such as D7P, PAD, and HAM, the domain-specific model matches state-of-the-art performance. In figure 5, we compute the utility (Newell and Deng, 2020) of the DINO and MONET model compared to the supervised pre-trained ImageNet model, measuring the saving in labels by the respective representations. Specifically, utility is the ratio of additional labels needed for the supervised pre-trained model to match the performance of the others. For most tasks, there is a significant benefit in using the representations from the DINO model compared to that of the domain-agnostic supervised one. On average across all downstream tasks, the DINO model reduces the necessary annotated samples by a factor of 2.

5. Conclusion

In this work, we have taken steps toward developing purely visual domain-specific foundation models for digital dermatology for scalable inference. Through a series of experiments across diverse diagnostic tasks, we demonstrated that dermatology-specific pre-training, particularly with methods such as DINO or iBOT, can outperform and are more label-efficient than models pre-trained on generic datasets like ImageNet. We specifically focused on smaller models and showed that they can achieve performance on par with or close to 50 times larger state-of-the-art models like MONET when subject to careful pre-training. These smaller models are more suitable for resource-limited clinical or teledermatology settings than the current state-of-the-art models, easing the adaptability for a broad range of clinically relevant use cases. While the models presented here show strong potential, further refinement in pre-training methodologies and expanding pre-training data to include more diverse populations and conditions will be essential for continued improvement. Additionally, exploring the trade-offs between model size and diagnostic performance would be valuable to further optimize the models' efficiency. By releasing the models and tools publicly, we hope to accelerate progress in the field of AI for dermatology, as these models can serve as a starting point for future applications and lower the need for annotated samples.

References

- Anmol Arora, Joseph E Alderman, Joanne Palmer, et al. The value of standards for health datasets in artificial intelligence-based applications. *Nature Medicine*, 2023.
- Muhammad Awais, Muzammal Naseer, Salman Khan, et al. Foundational Models Defining a New Era in Vision: A Survey and Outlook, July 2023.
- Bobby Azad, Reza Azad, Sania Eskandari, et al. Foundational models in medical imaging: A comprehensive survey and future vision. *arXiv preprint arXiv:2310.18689*, 2023.
- Elif Baykal, Hulya Dogan, Mustafa Emre Ercin, et al. Transfer learning with pre-trained deep convolutional neural networks for serous cell classification. *Multimedia Tools and Applications*, 2020.
- Mathilde Caron, Hugo Touvron, Ishan Misra, et al. Emerging properties in self-supervised vision transformers. In *Proceedings of the IEEE/CVF international conference on computer vision*, 2021.
- Daniel C. Castro, Ian Walker, and Ben Glocker. Causality matters in medical imaging. *Nature Communications*, 2020.
- Ting Chen, Simon Kornblith, Mohammad Norouzi, et al. A Simple Framework for Contrastive Learning of Visual Representations. In *Proceedings of the 37th International Conference on Machine Learning*. PMLR, 2020.
- Roxana Daneshjou, Kailas Vodrahalli, Roberto A. Novoa, et al. Disparities in dermatology AI performance on a diverse, curated clinical image set. *Science Advances*, 2022.
- Jia Deng, Wei Dong, Richard Socher, et al. Imagenet: A large-scale hierarchical image database. In *2009 IEEE conference on computer vision and pattern recognition*, pages 248–255. Ieee, 2009.
- Alexey Dosovitskiy. An image is worth 16x16 words: Transformers for image recognition at scale. *arXiv preprint arXiv:2010.11929*, 2020.
- I. Giotis, N. Molders, S. Land, et al. Med-node: A computer-assisted melanoma diagnosis system using non-dermoscopic images". *Expert Systems with Applications*, 2015.
- Philippe Gottfrois, Fabian Gröger, Herizo Andriambololoniaina, et al. Passion for dermatology: Bridging the diversity gap with pigmented skin images from sub-saharan africa. *MICCAI*, 2024.
- Jean-Bastien Grill, Florian Strub, Florent Altché, et al. Bootstrap Your Own Latent - A New Approach to Self-Supervised Learning. In *Advances in Neural Information Processing Systems*. Curran Associates, Inc., 2020.
- Fabian Gröger, Simone Lionetti, Philippe Gottfrois, et al. Towards reliable dermatology evaluation benchmarks. In *Machine Learning for Health (ML4H)*. PMLR, 2023.
- Fabian Gröger, Simone Lionetti, Philippe Gottfrois, Alvaro Gonzalez-Jimenez, Ludovic Amruthalingam, Labelling Consortium, Matthew Groh, Alexander A. Navarini, and Marc Pouly. Intrinsic Self-Supervision for Data Quality Audits.

- Advances in Neural Information Processing Systems (NeurIPS)*, 12 2024.
- Matthew Groh, Caleb Harris, Luis Soenksen, Felix Lau, Rachel Han, Aerin Kim, Arash Koochek, and Omar Badri. Evaluating deep neural networks trained on clinical images in dermatology with the fitzpatrick 17k dataset. In *IEEE/CVF Conference on Computer Vision and Pattern Recognition*, pages 1820–1828, 2021.
- Kaiming He, Xiangyu Zhang, Shaoqing Ren, et al. Deep residual learning for image recognition. In *Proceedings of the IEEE conference on computer vision and pattern recognition*, 2016.
- ISIC. ISIC Archive. www.isic-archive.com, 2016.
- Joseph Jacob, Olga Ciccarelli, Frederik Barkhof, and Daniel C Alexander. Disentangling human error from the ground truth in segmentation of medical images. *Advances in Neural Information Processing Systems*, 33:15750–15762, 2021.
- Jeremy Kawahara, Sara Daneshvar, Giuseppe Argenziano, et al. Seven-point checklist and skin lesion classification using multitask multimodal neural nets. *IEEE Journal of Biomedical and Health Informatics*, 2019.
- Chanwoo Kim, Soham U Gadgil, Alex J DeGrave, et al. Transparent medical image ai via an image-text foundation model grounded in medical literature. *Nature Medicine*, 2024.
- Xiao Liu, Fanjin Zhang, Zhenyu Hou, et al. Self-supervised Learning: Generative or Contrastive. *IEEE TKDE*, 2021. ISSN 1041-4347, 1558-2191, 2326-3865.
- Ming Y Lu, Bowen Chen, Drew FK Williamson, et al. A visual-language foundation model for computational pathology. *Nature Medicine*, 2024.
- Teresa Mendonça, Pedro M Ferreira, Jorge S Marques, et al. Ph 2-a dermoscopic image database for research and benchmarking. In *2013 35th annual international conference of the IEEE engineering in medicine and biology society (EMBC)*. IEEE, 2013.
- Alejandro Newell and Jia Deng. How useful is self-supervised pretraining for visual tasks? In *Proceedings of the IEEE/CVF Conference on Computer Vision and Pattern Recognition*, 2020.
- Andre G. C. Pacheco, Gustavo R. Lima, Amanda S. Salomão, et al. PAD-UFES-20: A skin lesion dataset composed of patient data and clinical images collected from smartphones. *Data in Brief*, 2020.
- Adam Paszke, Sam Gross, Francisco Massa, et al. Pytorch: An imperative style, high-performance deep learning library. *Advances in neural information processing systems*, 2019.
- Alec Radford, Jong Wook Kim, Chris Hallacy, et al. Learning transferable visual models from natural language supervision. In *International conference on machine learning*. PMLR, 2021.
- Saeed Shurrab and Rehab Duwairi. Self-supervised learning methods and applications in medical imaging analysis: A survey. *PeerJ Computer Science*, 2022.
- Xiaoxiao Sun, Jufeng Yang, Ming Sun, et al. A benchmark for automatic visual classification of clinical skin disease images. In Bastian Leibe, Jiri Matas, Nicu Sebe, and Max Welling, editors, *Computer Vision – ECCV 2016*. Springer International Publishing, 2016a.
- Xiaoxiao Sun, Jufeng Yang, Ming Sun, et al. A Benchmark for Automatic Visual Classification of Clinical Skin Disease Images. In Bastian Leibe, Jiri Matas, Nicu Sebe, and Max Welling, editors, *Computer Vision – ECCV 2016*. Springer International Publishing, Cham, 2016b.
- Hugo Touvron, Matthieu Cord, Alaaeldin El-Nouby, Jakob Verbeek, and Hervé Jégou. Three things everyone should know about vision transformers. In *European Conference on Computer Vision*, pages 497–515. Springer, 2022.
- Hugo Touvron, Thibaut Lavril, Gautier Izacard, et al. Llama: Open and efficient foundation language models. *arXiv preprint arXiv:2302.13971*, 2023.
- Philipp Tschandl, Cliff Rosendahl, and Harald Kittler. The HAM10000 dataset, a large collection of multi-source dermoscopic images of common pigmented skin lesions. *Scientific Data*, 2018.
- Chaoyi Wu, Xiaoman Zhang, Ya Zhang, et al. Towards generalist foundation model for radiology. *arXiv preprint arXiv:2308.02463*, 2023.

Sonnet Xu, Haiwen Gui, Veronica Rotemberg, et al. A framework for evaluating the efficacy of foundation embedding models in healthcare. *medRxiv*, 2024.

Jinghao Zhou, Chen Wei, Huiyu Wang, et al. iBOT: Image BERT Pre-Training with Online Tokenizer. *International Conference on Learning Representations (ICLR)*, 2022.

Yukun Zhou, Mark A Chia, Siegfried K Wagner, et al. A foundation model for generalizable disease detection from retinal images. *Nature*, 2023.

Appendix A. Pre-training Dataset

This section details the datasets used for pre-training. Public datasets without a license are under the public domain mark.

- **MED-NODE** (Giotis et al., 2015) features 170 clinical images for skin cancer detection by the University Medical Center Groningen, Netherlands (CC BY 4.0).
- **PH² Database** (Mendonça et al., 2013) features 200 dermoscopy images for melanocytic lesion classification by the Hospital Pedro Hispano in Matosinhos, Portugal.
- **Derm7pt** (Kawahara et al., 2019) features 2,022 dermoscopy and clinical images for skin condition diagnosis (CC BY-NC-SA 4.0).
- **SD-260** (Sun et al., 2016a) features 12,583 clinical images for skin condition diagnosis collected from DermQuest.
- **ISIC** (ISIC, 2016) features 107,208 dermoscopy images of pigmented skin lesions and features almost only low-pigmented skin (CC-BY-NC).
- A private collection of 119,858 clinical images reflecting the data distribution encountered in Swiss hospitals. Pictures were taken using diverse reflex cameras by trained photographers, anonymized, and used with approval EKNZ-2018-01074 from an ethical committee according to Swiss regulations.

Appendix B. Downstream Tasks

This section lists the suite of datasets used for evaluation. Bold indicates the respective downstream tasks.

- **MED-NODE (MED)** (Giotis et al., 2015) features 170 clinical images for skin cancer detection by the University Medical Center Groningen, Netherlands (CC BY 4.0). The images are categorized into melanoma and naevus.
- **PH² Database (PH2)** (Mendonça et al., 2013) features 200 dermoscopy images for melanocytic lesion classification by the Hospital Pedro Hispano in Matosinhos, Portugal. The images are categorized into common nevi, atypical nevi, and melanomas.
- **DDI** (Daneshjou et al., 2022) features 656 clinical images for skin cancer detection and rare disease classification by the Stanford Clinics (Stanford’s University dataset research agreement). The images are categorized into benign or malignant lesions (**DDI-M**).
- **Derm7pt (D7P)** (Kawahara et al., 2019) features 2,022 dermoscopy and clinical images for skin condition diagnosis (CC BY-NC-SA 4.0). The images are categorized into 16 diagnoses.
- **PAD-UFES-20 (PAD)** (Pacheco et al., 2020) features clinical images captured by smartphones (CC BY 4.0 license). The dataset consists of 1,373 patients, 1,641 skin lesions, and 2,298 images for six disease diagnoses.
- **PASSION** (Gottfrois et al., 2024) features 4,901 clinical images of 1,653 pigment-rich patients from Sub-Saharan countries (CC BY-NC 4.0 license). The dataset is categorized into the four common pediatric conditions (**PAS-C**) and impetigo cases (**PAS-I**).
- **SD-128 (SD1)** (Sun et al., 2016b) features 5,619 clinical images for skin condition diagnosis collected from DermQuest. The images are categorized into 123 diseases.
- **HAM10000 (HAM)** (Tschandl et al., 2018) features of 10,015 dermatoscopic images collected from different populations and institutions for seven diagnostic categories of pigmented lesions (CC BY-NC 4.0).

- **Fitzpatrick17k** (Groh et al., 2021) features 16,577 clinical images (CC BY-NC-SA 3.0). The dataset’s conditions are separated into three different granularity levels: high (**FST-H**), mid (**FST-M**), and low (**FST-L**).

Appendix C. Hyperparameters

Table 1 details the hyperparameters for the pre-training methods used to train the respective foundation models.

Appendix D. Detailed Results

Table 2 details the results from the frozen evaluation on the suite of downstream tasks. Consult Appendix B for details on downstream tasks and section 4 for the discussion on the results. Additionally, figure 3 visualizes both kNN and linear performance, similarly as done for figure 1.

Figure 4 shows the evaluation in low-data scenarios with linear classifiers, similar to figure 2. Figure 5 visualizes the utility of the representations for both kNN and linear evaluation in low-data scenarios as discussed in section 4.

Appendix E. PyPi Package

All checkpoints are released to make the foundation models widely available, and a dedicated package has been developed, enabling quick loading and instantiation of a foundation model to be used for downstream tasks. The package can be installed using `pip` via and will be released after the decision:

```
pip install self-supervised-dermatology
```

Afterward, the package can be imported and used to obtain the pre-trained models, which can be used as PyTorch models.

```
from self-supervised-dermatology import Embedder
```

```
model = Embedder.load_pretrained('SimCLR')
model = Embedder.load_pretrained('BYOL')
model = Embedder.load_pretrained('DINO')
model = Embedder.load_pretrained('iBOT')
```

```
rand_img = torch.rand(1, 3, 224, 224)
embedding = model(rand_img)
```


Table 1: Hyperparameters used for each SSL method, where “n.a.” indicates that this parameter is not used.

Hyperparameter	SimCLR	BYOL	DINO	iBOT
Encoder	ResNet-50	ResNet-50	ViT-T	ViT-T
Batch size	640	60	260	224
Epochs	100	100	100	100
Optim	Adam	Adam	AdamW	AdamW
Learning rate (lr)	0.00003	0.003	0.0005	0.005
Min. lr.	1e-6	1e-6	1e-6	5e-4
Warmup epochs lr.	10	10	10	10
Weight decay (wd)	1e-6	n.a.	0.04	0.04
Weight decay end	0.4	n.a.	0.4	0.4
Use lr. scheduler	True	True	True	True
Use wd. scheduler	True	False	True	True
Momentum teacher	n.a.	0.996	0.9995	0.996
Global crops scale	n.a.	n.a.	(0.7, 1.)	(0.7, 1.)
Local crops scale	n.a.	n.a.	(0.05, 0.4)	(0.05, 0.4)
N.o. global, local crops	n.a.	n.a.	(2, 12)	(2, 12)

Table 2: Macro-averaged test F1 scores of pre-trained models for twelve dermatology diagnostic tasks. Bold values correspond to the best scores. ANOVA was used to compare the mean F1 scores across multiple models, followed by Tukey’s post-hoc test to identify significant pairwise differences ($p < 0.05$) denoted with a *.

Pre-training	Dataset	Architecture	MED		PH2		DDI-M		D7P	
			lin.	kNN	lin.	kNN	lin.	kNN	lin.	kNN
Supervised	ImageNet	ResNet-50	84.5 ± 2.9	64.6 ± 2.1	61.0 ± 4.0	47.7 ± 7.1	50.3 ± 3.2	39.1 ± 0.9	32.6 ± 1.0	19.9 ± 1.7
Supervised	ImageNet	ViT-T/16	84.4 ± 0.9	71.1 ± 3.9	63.5 ± 2.8	58.2 ± 5.7	49.6 ± 3.2	37.7 ± 2.7	32.8 ± 1.5	22.4 ± 1.8
MONET	Derma Lit.	ViT-L/14	87.2 ± 2.6	71.9 ± 2.8	70.2 ± 1.3	65.3 ± 4.9	56.9 ± 5.7	44.7 ± 1.9	45.5 ± 2.3*	30.3 ± 1.2
SimCLR	Derma Img.	ResNet-50	75.0 ± 0.0	71.4 ± 4.5	32.9 ± 1.9	50.8 ± 3.1	0.0 ± 0.0	31.2 ± 1.6	3.9 ± 0.1	15.3 ± 2.1
BYOL	Derma Img.	ResNet-50	77.4 ± 3.1	67.5 ± 3.8	35.0 ± 3.0	60.2 ± 6.9	0.0 ± 0.0	29.3 ± 3.6	7.2 ± 0.1	21.7 ± 0.8
DINO	Derma Img.	ViT-T/16	87.0 ± 2.3	71.4 ± 2.2	67.4 ± 3.3	64.1 ± 1.8	39.7 ± 3.0	43.5 ± 4.3	35.6 ± 0.9	28.8 ± 1.8
iBOT	Derma Img.	ViT-T/16	88.7 ± 2.0	77.5 ± 4.3	61.7 ± 2.3	61.8 ± 4.0	42.4 ± 5.0	38.2 ± 5.5	31.3 ± 1.7	26.1 ± 1.1
Pre-training	Dataset	Architecture	PAD		PAS-C		PAS-I		SD1	
			lin.	kNN	lin.	kNN	lin.	kNN	lin.	kNN
Supervised	ImageNet	ResNet-50	55.4 ± 1.0	40.4 ± 1.8	56.9 ± 0.0	55.8 ± 0.3	87.1 ± 0.0	44.5 ± 0.8	46.2 ± 0.3	39.0 ± 0.5
Supervised	ImageNet	ViT-T/16	51.7 ± 1.6	35.1 ± 1.4	58.0 ± 0.0	52.9 ± 0.2	90.0 ± 0.0	42.0 ± 0.5	42.6 ± 0.3	37.3 ± 0.6
MONET	Derma Lit.	ViT-L/14	60.8 ± 1.4	45.6 ± 1.4	69.9 ± 0.0*	63.5 ± 0.1*	91.0 ± 0.0*	57.7 ± 0.8*	62.9 ± 0.5*	51.2 ± 0.8*
SimCLR	Derma Img.	ResNet-50	18.0 ± 0.5	28.6 ± 1.7	27.6 ± 0.0	40.0 ± 0.2	88.8 ± 0.0	29.8 ± 0.6	0.1 ± 0.0	16.2 ± 0.3
BYOL	Derma Img.	ResNet-50	30.1 ± 0.9	34.9 ± 1.4	52.2 ± 0.0	54.5 ± 0.4	88.8 ± 0.0	44.6 ± 1.0	3.9 ± 0.3	39.0 ± 1.1
DINO	Derma Img.	ViT-T/16	51.9 ± 1.7	44.2 ± 1.9	52.0 ± 0.6	51.9 ± 0.4	88.9 ± 0.2	43.9 ± 1.5	45.3 ± 0.5	46.9 ± 0.4
iBOT	Derma Img.	ViT-T/16	50.6 ± 1.4	39.5 ± 0.5	49.1 ± 0.6	50.1 ± 0.6	88.4 ± 0.2	43.8 ± 1.1	44.9 ± 0.8	46.4 ± 0.6
Pre-training	Dataset	Architecture	HAM		FST-H		FST-M		FST-L	
			lin.	kNN	lin.	kNN	lin.	kNN	lin.	kNN
Supervised	ImageNet	ResNet-50	57.2 ± 0.0	43.3 ± 0.3	61.1 ± 0.2	67.2 ± 0.4	45.0 ± 1.1	52.6 ± 0.8	39.7 ± 0.5	40.1 ± 0.4
Supervised	ImageNet	ViT-T/16	54.7 ± 0.0	34.6 ± 0.3	58.6 ± 0.4	65.7 ± 0.6	42.8 ± 0.9	49.3 ± 0.6	33.4 ± 0.8	37.4 ± 0.6
MONET	Derma Lit.	ViT-L/14	64.4 ± 0.0*	43.4 ± 0.2	71.2 ± 0.2*	76.0 ± 0.6*	59.8 ± 0.4*	64.7 ± 1.0*	55.0 ± 0.4*	51.1 ± 0.2*
SimCLR	Derma Img.	ResNet-50	15.4 ± 0.0	28.0 ± 0.5	30.1 ± 0.2	49.7 ± 0.3	8.8 ± 0.0	29.3 ± 0.8	0.3 ± 0.0	18.9 ± 0.3
BYOL	Derma Img.	ResNet-50	28.8 ± 0.0	41.0 ± 0.4	45.9 ± 0.3	66.1 ± 0.4	17.3 ± 0.2	52.0 ± 0.9	3.9 ± 0.1	39.1 ± 0.3
DINO	Derma Img.	ViT-T/16	57.3 ± 0.8	46.3 ± 0.2*	55.0 ± 0.2	68.0 ± 0.5	36.5 ± 0.5	56.0 ± 0.2	32.3 ± 0.6	42.9 ± 0.6
iBOT	Derma Img.	ViT-T/16	57.9 ± 0.7	42.0 ± 0.5	53.6 ± 0.3	68.5 ± 0.6	33.8 ± 0.9	55.8 ± 0.6	29.8 ± 0.5	42.8 ± 0.3

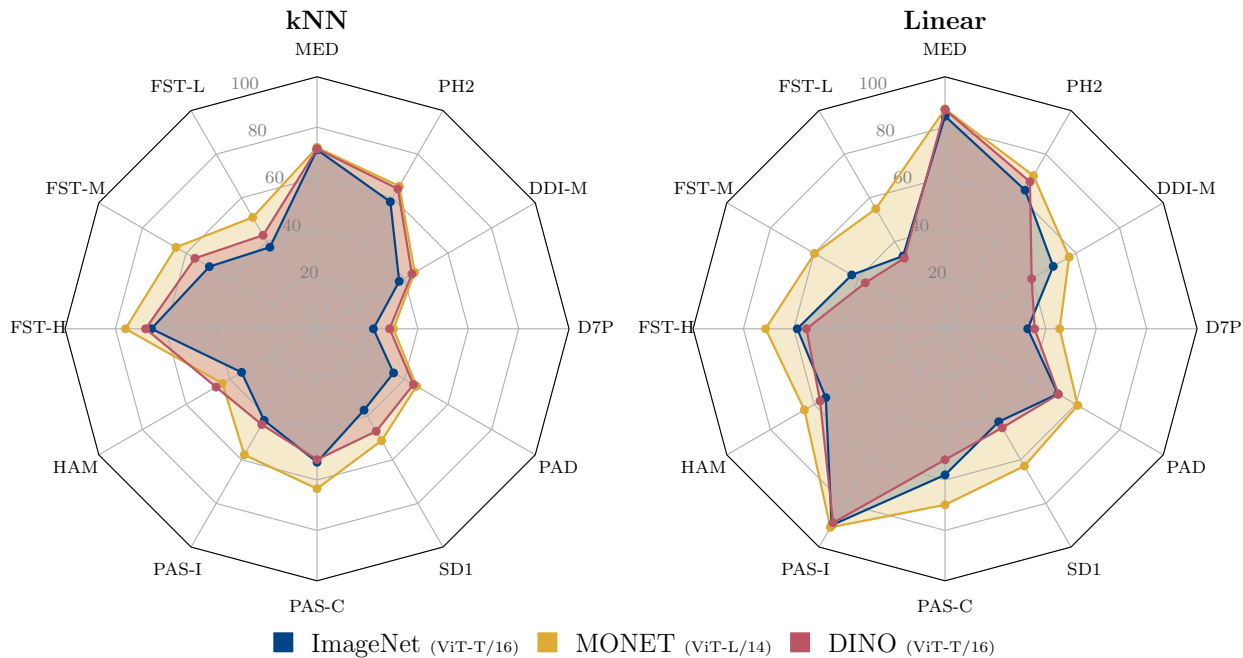


Figure 3: Macro-averaged test F1 for frozen kNN and linear evaluation of the best-performing foundation model, domain-agnostic ImageNet model, and MONET for dermatological diagnostic tasks. Consult Appendix B for task details and D for more detailed results.

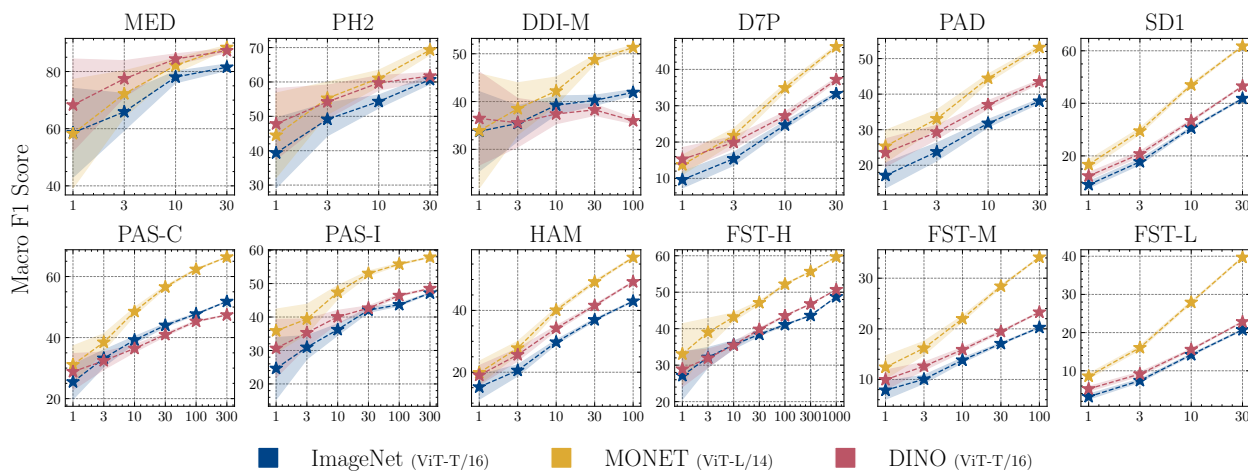
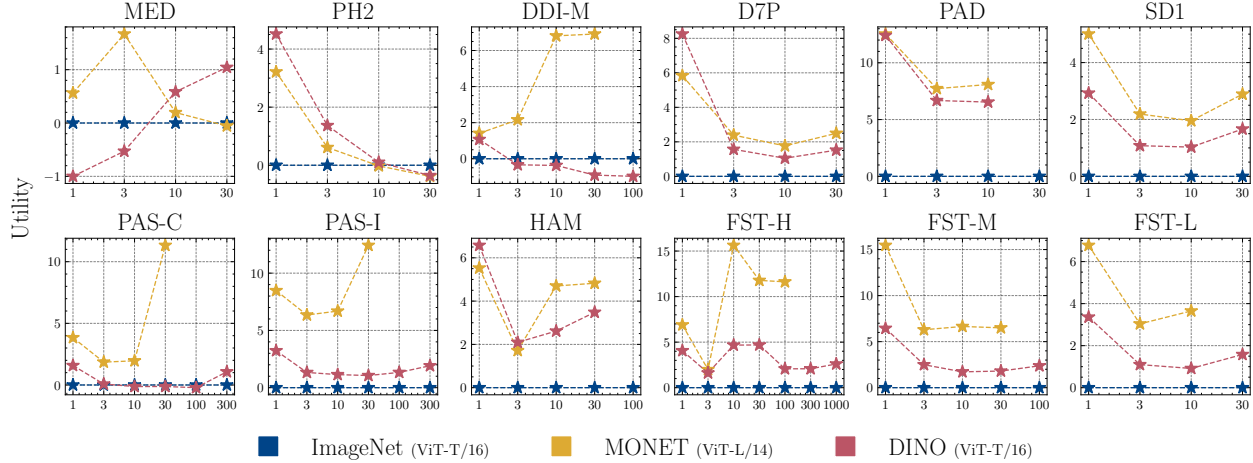
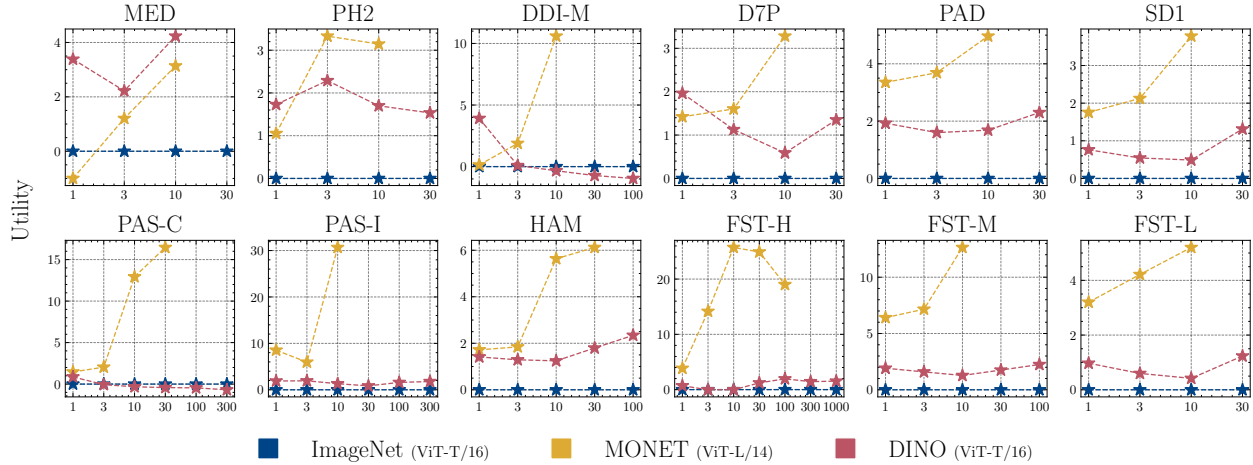


Figure 4: Results of a linear classifier on pre-trained representations when varying the number of training samples per class available for downstream tasks. Performance is obtained by repeating the sampling process 50 times and reporting the average and standard errors.

(a) k -Nearest neighbor classifiers

(b) Linear classifiers

Figure 5: Utility score (Newell and Deng, 2020) of the kNN and linear classifiers on pre-trained representations of MONET and DINO from figures 2 and 4 compared against those from a supervised pre-trained ViT-T on ImageNet. Utility quantifies the effectiveness of the representations as the saving in labels. Specifically, to achieve the same accuracy with other representations, the ratio of how many more labels would be needed. It is positive if there is a benefit, negative if there is a drawback, zero if there is no difference in using the representations, and infinite when there is not any number of labeled samples such that the performance matches.